

On the use of two emerging laser-based flaw-detection techniques – Considerations and practicalities

D. Vangi^a, M.S. Gulino^{a,*}, N. Montinaro^{b,c}, C. Mineo^d, D. Cerniglia^b, G. Epasto^e

^a Department of Industrial Engineering, Università degli Studi di Firenze, Via di Santa Marta 3, Firenze 50139, Italy

^b Department of Engineering, Università degli Studi di Palermo, Viale delle Scienze Edificio 8, Palermo 90128, Italy

^c Institute for Advanced Energy Technologies (ITAE), National Research Council, Viale delle Scienze Edificio 9, Palermo 90128, Italy

^d Institute for High Performance Computing and Networking, National Research Council, Via Ugo La Malfa 153, Palermo 90146, Italy

^e Department of Engineering, Università degli Studi di Messina, Contrada di Dio, Sant'Agata, Messina 98166, Italy

ARTICLE INFO

Keywords:

Ultrasonics
Laser-acoustics
Interferometry
Deflectometry
Ndt

ABSTRACT

The pursuit of non-contact techniques for detecting ultrasonic waves propagating on the surface of solids is stimulated by the possibility of gaining some advantages over conventional contact methods. Non-contact methods are becoming a milestone in performing non-destructive evaluation in several industrial fields, where hazardous environments, narrow spaces, high temperatures, and complex geometries are encountered. Such methods exploit photo-acoustic interactions between light and sound waves. This work compares two non-contact laser-based methods for detecting artificial flaws of different sizes in metallic specimens. It uses multi-signal homodyne interferometry and single beam deflectometry to record the ultrasonic waves produced by a piezoelectric probe capable of generating surface Rayleigh waves. The results were analysed in both time and frequency domains. Moreover, the signal-to-noise ratio was evaluated for both measurement systems by changing the distance between the defect and the point where the signals were collected. The results show the main differences between the two techniques and the practicalities associated with their usage. The employed refractometric method has a lower sensitivity to surface roughness than the interferometric method. On the other hand, the interferometric technique allows for higher spatial resolution, wider frequency bandwidth and a higher detectable frequency (i.e., detecting low-sized defects).

1. Introduction

Non-destructive evaluation through non-contact ultrasonic techniques is becoming relevant in all fields of industrial engineering to detect flaws, fatigue cracks and corrosive effects on mechanical components. The growth of non-contact ultrasonic techniques is mainly related to practical aspects, such as the possibility of eliminating couplant media, carrying out inspections in hazardous environments, narrow spaces, high-temperature fields, and components having complex geometries [1,2]. Generally, non-contact techniques are divided based on the detection method [3]: capacitive [4], gas coupling [5], and laser ultrasound [6]. An emerging non-contact detection technique is the Gas-Coupled Laser Acoustic Detection (GCLAD) method [7].

Non-contact detection of ultrasound allows measuring ultrasonic waves through optical methods, exploiting photo-acoustic interaction phenomena involving light and sound waves [8]. Ultrasound detection by optical methods has had vigorous development since the 1970s. It allows obtaining high acquisition rates per surface unit compared to

piezoelectric probes. Moreover, optical methods show insensitivity to electromagnetic interference and wide bandwidth for different applications, from biomedical to industrial fields [9]. Optical methods are mainly based on interferometry, declining in different application techniques [6,10–17]. They include optical heterodyning and homodyning, differential interferometry, and velocity or time-delay interferometry. Interferometric methods detect the variations in the optical interference patterns induced by the specimen surface's displacements due to the ultrasonic wave passage [18].

Besides these main techniques, other optical techniques based on deflectometry have been developed. These methods use the photoelastic principle, i.e., they measure the refractive index variation in a medium due to the passage of the pressure wave. The variation of the refractive index is detected through the variations in intensity (Intensity-sensitive detection of refractive index), deflection angle (single beam deflectometry), in the phase of a laser beam which passes through a medium (Phase-sensitive ultrasound detection) or in the reflection index (fibre Bragg grating sensor) [9,10,19–24].

* Corresponding author.

E-mail address: michelangelosanto.gulino@unifi.it (M.S. Gulino).

Amongst non-contact ultrasonic techniques, optical detection is currently applied for non-destructive evaluation through laser ultrasonics, including interferometry or deflectometry approaches [9]. It has been demonstrated to be suitable for producing high-resolution scans [1]. Furthermore, it can be helpful when rotating components have to be inspected [25–27] or for remote control. Non-contact laser methods have been used to obtain automated crack detection and diagnosis in an aluminium [28] and steel plates [29], to evaluate debonding in composites [30] and to investigate thickness reduction in pipelines [31]. In the scientific literature, few works are comparing interferometric and refractometric techniques [9,32], with the former currently being used more in non-destructive evaluation.

This work uses the GCLAD method and the multi-signal homodyne interferometry. The former belongs to the methods based on deflectometry, and in particular, it is a single-beam deflectometry method. The method is different to the Laser beam deflection technique [19] because the laser does not directly interfere with the surface of the specimens, where the ultrasonic waves have to be detected. In the case of the GCLAD technique, the laser beam detects changes in the refractive index in the air surrounding the specimen due to the refraction of ultrasonic waves in the air. The first studies on the GCLAD technique date back to the 1990s [33,34]. In terms of frequency response and sensitivity, its features were highlighted in [7,35,36]. Subsequently, its applicability to non-destructive testing on composite [37] and metallic [34,38–42] materials has been evaluated. Although its applicability to non-destructive testing has been widely demonstrated, the technique is still developing, as there are no comparisons with more established techniques and industrial applications. In particular, a comparison with non-contact techniques - as the optical interferometric ones - appears to be interesting, considering that these latter ones have instead found many applications in the industrial field [43].

A multi-signal homodyne interferometer is used in this work. That is an interferometry device called Quartet, commercialised by Sound & Bright. The device combines the advantages of homodyne interferometry and the ability to be sensitive to optical speckles [44,45], making it suitable for measuring ultrasound waves on rough surfaces.

The multi-signal homodyne interferometry and the GCLAD technique have limitations that must be considered. Homodyne interferometric detection relies on the beat between a relatively robust local oscillator (LO) field at the carrier frequency and a signal beam with sidebands centred around the carrier frequency. This type of signal detection, or signal readout, is widely used in quantum optics applications and has also been used in advanced interferometric gravitational wave detectors [46]. The beam jitter noise, the electronic noise of the photodetectors, and the LO intensity noise can limit the homodyne detection at sound/ultrasound frequency bands [47]. However, the biggest drawback of interferometric ultrasonic wave measurement is that the laser beam needs to impinge the surface where one intends to detect the wave. Although this allows a precise and punctual measurement, the local surface roughness strongly affects the signal-to-noise ratio (SNR) [48]. The light scattering due to the rough surface is a discussed argument [49,50]. The surface roughness effect on interferometric detection has recently made a comeback as the main issue in inspecting additive manufactured parts, where roughness can be very high compared to the machined ones. In [51], the application of laser ultrasonic inspection with interferometric detection has been evaluated for a Wire Arc Additive Manufactured part. The specimens produced by this technology, without surface machining, have very high roughness. In this paper, the authors found it difficult to detect the defect echo in the A-scan plots due to the low SNR of the recorded signals. Nonetheless, defect detection can be successful by analysing the B-scan plots. Another paper [52] deals with the application of the laser ultrasonic technique on specimens produced by laser powder deposition. The authors detected near-surface defects of about 0.1 mm in diameter on rough specimens. It is also worth mentioning that optical methods based on interferometric detectors can be minia-

turised without losing sensitivity, which is not possible for piezoelectric probes [9].

The GCLAD method can be employed in different experimental configurations [7], as it always detects the ultrasound wave along a line, coinciding with the probe laser beam. This aspect can be advantageous for inspections of planar components in order to speed up the inspection on a line, allowing a scan of the object in only one direction [41,42]. However, this feature can be a disadvantage when a flexible measurement is required. This limitation can be partially overcome by adopting experimental configurations that focus the laser beam on a small area, as indicated in [39]. In order to obtain high sensitivity, such a method requires a small diameter, a limited divergence, and a high length of the laser beam probe [7], which is not always applicable to all geometries. The bandwidth is determined by the photodiode's rise time and the probing laser beam diameter [7]. The smaller the beam diameter, with respect to the acoustic wavelength, the greater the obtainable bandwidth. For example, by detecting refractive index changes in water with a laser beam diameter of 90 μm , a theoretical bandwidth of 17 MHz is obtained [53]. Using the technique in the air, with a laser beam of 1 mm in diameter, a band of just over 1 MHz is typically obtained.

Currently, no devices on the market use the GCLAD technique. Thus, it is necessary to set up a detection system consisting of a photodiode and its electronics in the laboratory. SNR, bandwidth, and sensitivity can differ depending on the electronics and the laser.

2. Theoretical background

2.1. Multi-signal homodyne interferometry

A laser beam reflected by a rough sample surface generates many optical speckles. In a speckle-based acquisition instrument, the beam is combined with the interferometer reference beam and focused on a photodetector array. Each array detector collects a few speckles and delivers a homodyne signal. The detectors produce a time-varying analogue voltage proportional to the rectified instantaneous surface displacement at ultrasonic frequencies. A speckle-based interferometer with a photodetector array made out of fifty elements is used in the current work. The latter can detect ultrasonic waves in various environments, mitigating the loss in sensitivity on rough surfaces. Fig. 1a presents a schematic representation of how the adopted instrument works. The laser beam generated by the internal laser passes through multiple optics within

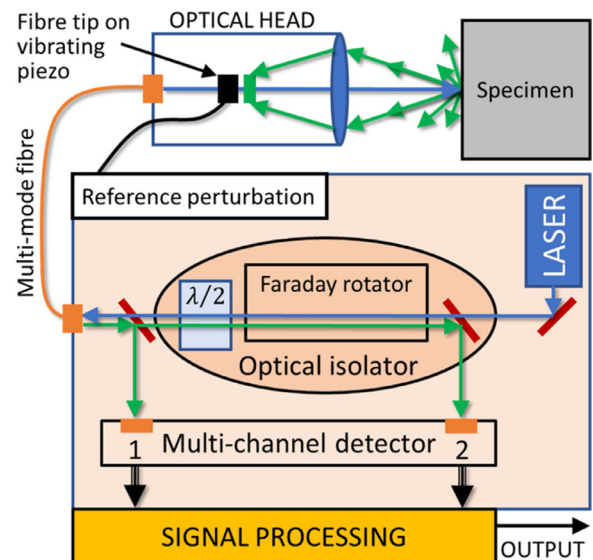


Fig. 1. Schematic representation of the interferometric instrument [47,48] used in this work.

the receiver before being focused on a multimode fibre. Around 4–5% of the light is reflected towards the receiver at the end of the fibre due to a natural optical phenomenon, while the rest is focused on the sample. The diffuse light reflected by the sample surface is then collected by a large lens at the front of the optical head, maximising the number of speckles gathered for signal processing. The speckled beam then travels through the optical fibre, interfering with the previously mentioned 4–5% partial reflection. It is important to note that the light polarisation components are scrambled while travelling back through the multimode fibre. Once back in the system, the beam travels through a first Polarised Beam Splitter (PBS), isolating the vertical polarisation component and directed towards one of the two detector arrays. The rest of the beam travels through an Optical Isolator consisting of a Faraday rotator and a PBS. This second PBS sends the vertical (previously horizontal) returning signal beam component towards the second Multi-Channel Detector. Each homodyne signal is processed in parallel using a signal processing architecture based on a random quadrature demodulation scheme, taking advantage of the random phase distribution inherent to speckle light. Because of the random nature of each of the fifty detected signal phases, the instrument is designed to perform signal rectification without consideration of phase.

The instrument's electronic processing allows single-shot measurements on fast-moving objects thanks to signal filtering based on rectified demodulation. It reduces the signal noise and improves the acquisition of small displacements in high-frequency ranges.

2.2. Single beam deflectometry

When an ultrasonic wave propagating inside a material reaches the interface with air or other fluid (for example, water for immersion tests), diffraction of the wave will occur. Consequently, according to Snell's law, part of the acoustic energy propagates in the gas (or fluid), and the refracted wave will modify the medium refractive index. If a laser beam crosses the affected region of the medium, deviations and displacements in the direction of the beam can be observed and are proportional to the pressure gradient in the medium [25,34]. The displacement of the laser beam (Δz) is detected with a photodiode, which allows obtaining an output voltage modulated based on the displacement over time. The geometric parameters that describe the system's response are represented in Fig. 1, where x_s represents the length of the perturbed region crossed by the laser beam and x_1 the distance from the photodiode. The higher the values of these parameters, the greater the laser beam displacement at the photodiode.

Another critical parameter is the beam's diameter relative to the medium's acoustic wavelength. Indeed, the beam deflection depends on the acoustic pressure gradient, and the overall displacement is an average of the displacements within the beam section. The smaller the diameter of the laser beam, the more uniform the extent of the gradient crossed by the light beam. Conversely, a large beam will mediate its displacement between areas with gradients of opposite signs. It also implies that a small acoustic wavelength with the same laser beam diameter will produce a smaller displacement than a large wavelength. That causes a frequency filter effect, whereby the high frequencies are less amplified than the low ones. For example, the propagation of the diffracted wave in water, which has a higher propagation speed than air, produces a much greater sensitivity.

Different experimental configurations can be used based on the diagram in Fig. 2. The most common configurations are those shown in Fig. 3, particularly suitable for detecting Rayleigh waves in a specimen.

In configuration A, the laser beam probe is parallel to the part surface. The length of the beam affected by the perturbation (x_s) is equal to the width of the wavefront in the air. In this case, the distance of the beam from the surface can also be minimal, minimising the attenuation phenomena of the acoustic wave in the air. In configuration B, the laser beam is aligned to the direction of acoustic wave propagation on the specimen surface, and the beam is inclined by the angle of refraction

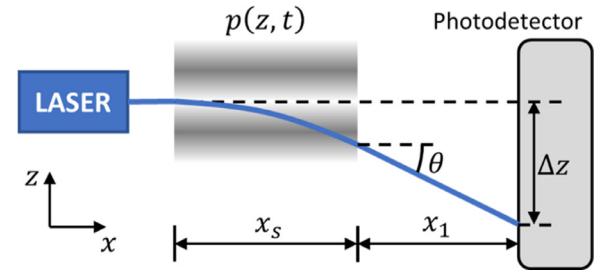


Fig. 2. Schematic working principle of the GCLAD technique used in this work.

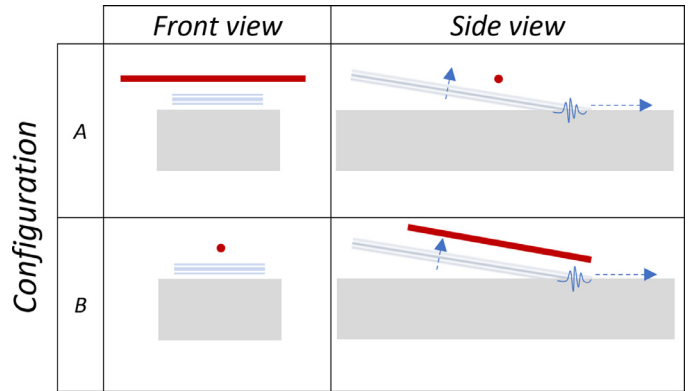


Fig. 3. Possible GCLAD experimental configurations for detecting the refraction in the air of Rayleigh waves that propagate on a component surface.

in the air. This way, the laser beam propagates in a plane parallel to the wavefront to capture a constant pressure gradient along its entire path. In this configuration, x_s can be high, but the distance of the beam from the piece is not constant, and the attenuation of the wave for large distances decreases the sensitivity of the method. From this point forward, configurations A and B of GCLAD are abbreviated respectively with GCLAD-A and GCLAD-B for conciseness. In GCLAD-B, the system is very selective, similarly to the probes coupled in the air, i.e., only the waves propagating perpendicular to the laser beam are detected, while the others are not detected. In GCLAD-A, on the other hand, the system can detect all the waves regardless of their propagation angle. Therefore, the GCLAD configuration must be chosen based on the geometry of the piece and the space available around it to maximise sensitivity.

3. Materials and methods

3.1. Samples

In order to perform a comparison between the interferometric technique and the GCLAD one, ten specimens were produced. Such specimens are 582 mm long, 70 mm wide, and 12 mm thick plates made of S235 steel. Electric discharge machining (EDM) was used to introduce artificial defects on the sample surface. The width and depth of the defects are different, as reported in Table 1, while the width is the same (0.8 mm, compatible with the size of the EDM electrode). The defects' position is depicted in Fig. 4: the direct Rayleigh wave reaches the detection position and then the defect, whose flanks reflect most of the ultrasonic energy; the remaining part travels up to the backwall (BW) and is then reflected once again.

Table 1

Defects dimensions for the samples on which each defect has been generated.

h (mm)	1	3	6							
w (mm)	10	20	30	10	20	30	40	10	20	30

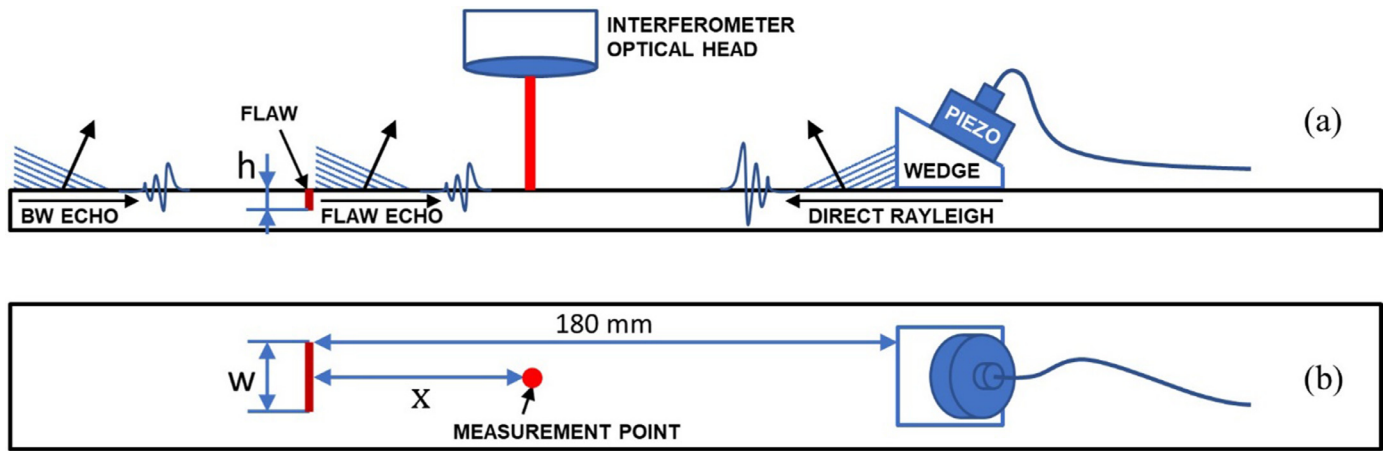


Fig. 4. Schematic view of the specimens. Side view (a) and top view (b). The measurement point represents where the laser beam was focused on the sample surface to collect the interferometric signals.

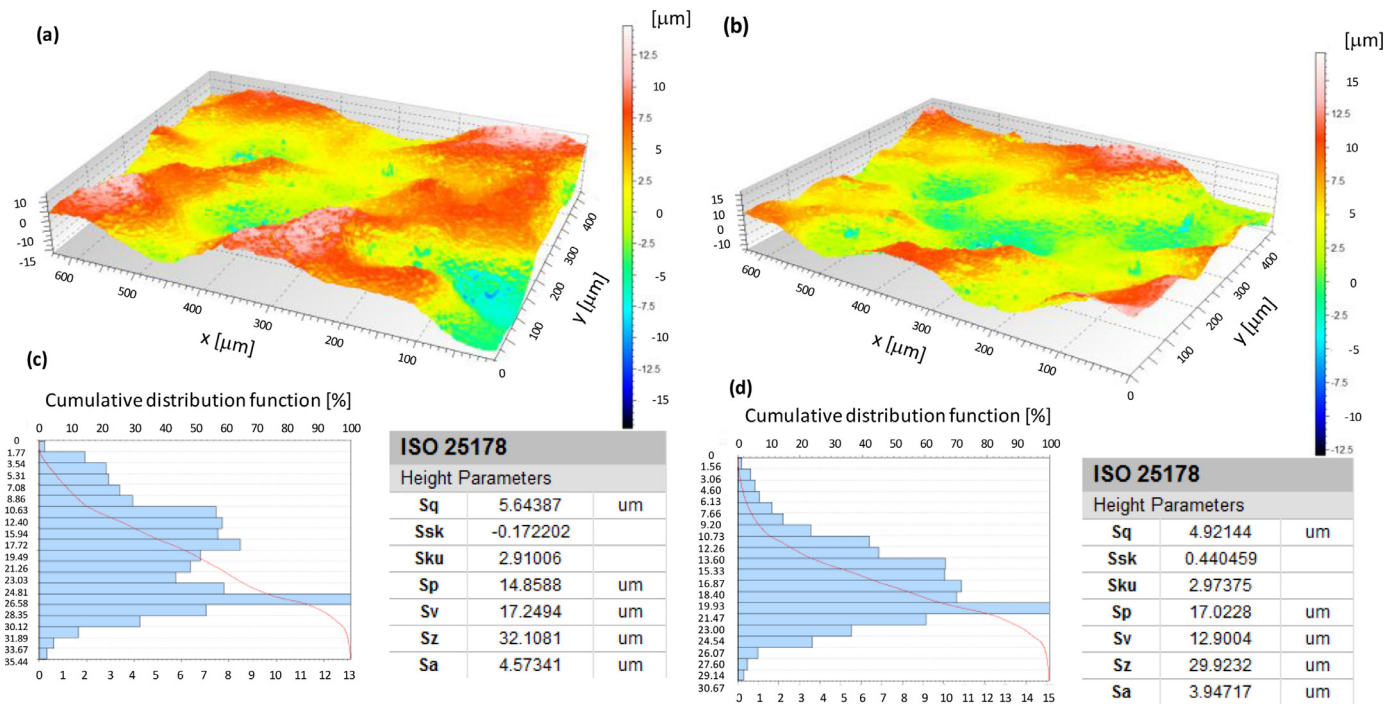


Fig. 5. Profile maps of the surface in two zones of a specimen (a)-(b) and related histograms of the surface texture (c)-(d).

It is worth mentioning that, apart from the introduction of artificial flaws, the specimens were left as received (i.e., no superficial treatment was carried out). The samples' surface presented partial oxidation. The roughness measurements were performed with a confocal microscope (Leica DCM 3D) that, by scanning the sample over its surface, generates a profile map over two zones of the same specimen (see Figs. 5a and 5b). In Figs. 5c and 5d the histograms of the two different zones show that the surface texture has peaks and valley mainly in the range $\pm 5 \mu\text{m}$. The average surface roughness S_a is $4.2 \mu\text{m}$. The data reported in Fig. 5 are extracted from the surfaces according to ISO 25,178 and are the following: S_q is the root mean square height of the surface, S_{sk} is the skewness of height distribution, S_{ku} is the kurtosis of height distribution, S_p is the maximum height of peaks, S_v is the maximum height of valleys, S_z is the maximum height of the surface and S_a is the arithmetical mean height of the surface.

The samples are nominally identical in terms of surface roughness because they have been obtained by cutting a single hot rolled 5900 mm-long plate.

The ultrasonic waves within the specimen were generated by a Panametrics piezoelectric probe, having a centre frequency of 500 kHz, a bandwidth of 600 kHz and a diameter of 25.4 mm. The probe was mounted over a sloped wedge allowing for the generation of surface Rayleigh waves. When propagating in the specimen, the waves were partially reflected by the defect and the bottom wall of the piece. At the same time, the diffraction of the waves in the air, with an angle of about 6.7° , occurred. Such a contact probe was chosen since it allows the generation of repeatable signals (assuming the probe remains perfectly coupled and stationary) and has a specific frequency. The measurements were performed by detecting both the direct wave and the echo due to the defect.

3.2. Measurement setups

The interferometer optical head, represented in Fig. 1, was equipped with a 50 mm focal distance lens. The Rayleigh wave was generated using the 500 kHz piezoelectric transducer and perspex wedge repre-

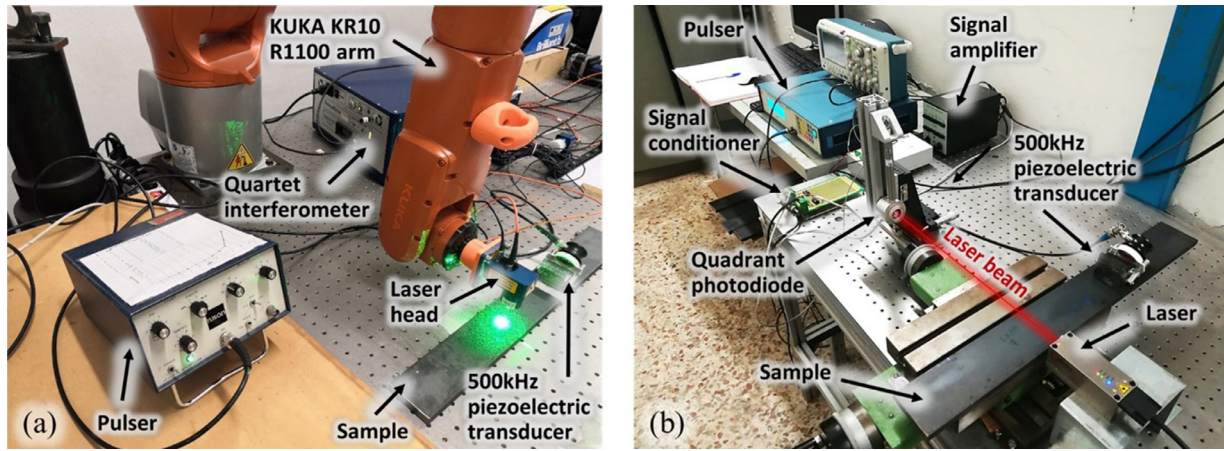


Fig. 6. Experimental setups. Interferometric measure (a) and GCLAD-A measure (b).

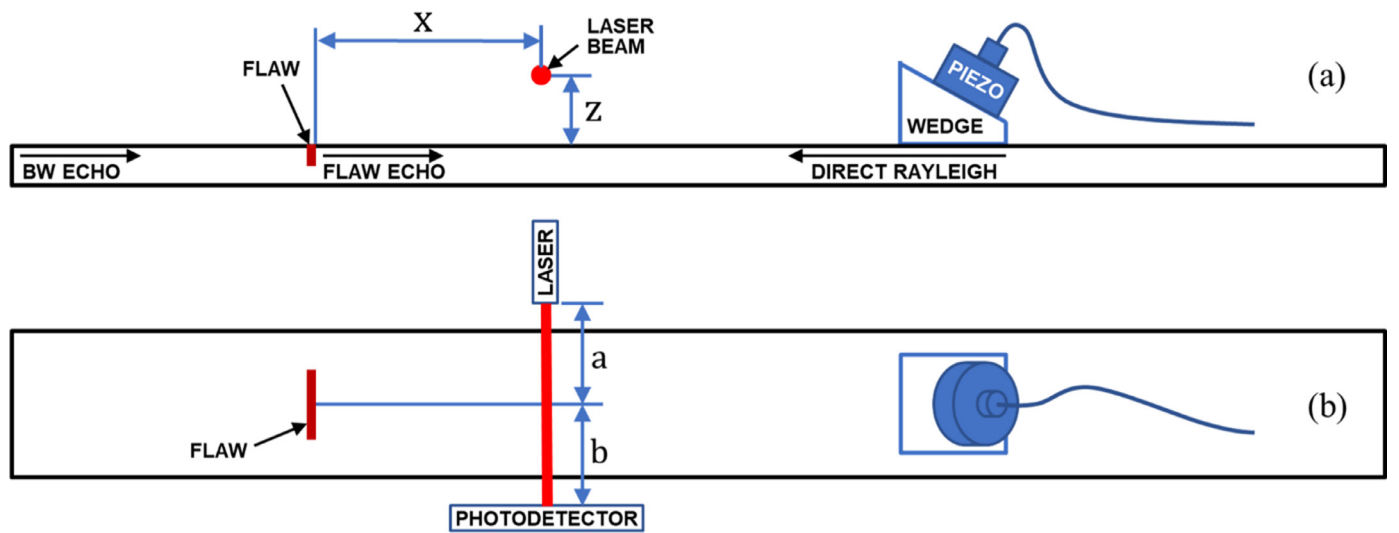


Fig. 7. Schematic representation of the experimental setup used for GCLAD-A. Side view (a) and top view (b).

sented in Fig. 4. Couplant gel was used to couple the transducer with the wedge and the wedge with the sample surface. The transducer was excited through a UT signal generator (NUSON model HF400). A KUKA KR10 R1100 was used to bring the interferometer optical head to the measurement point and apply minor adjustments to the position to maximise the signal level. Since the surface roughness of the samples influenced the SNR of the interferometric signal, it was deemed worthwhile to acquire multiple signals and average them to obtain a better final signal. As a rule of thumb, the sample-to-lens distance was iteratively adjusted to get at least the 40% of the maximum achievable signal. In practice, due to the surface variability of the specimens, the calibration fluctuated in the 40–60% range for all acquisitions. The final signals were obtained by averaging 1000 signals taken at each location. The instrument oscilloscope impedance was set to 50 Ω . Fig. 6a shows the setup used for the interferometric measures.

Signal detection by the GCLAD equipment was carried out in both GCLAD-A and GCLAD-B. A picture of the laboratory setup is given in Fig. 6b for GCLAD-A. The schematic representation for this configuration is depicted in Fig. 7. The distance between the artificial flaw and the laser beam (x) was set to different values, while the distance between the laser beam and the specimen surface (z) was 3 mm. The distance between the laser source and the specimen's longitudinal centerline (a) was 60 mm, and the distance between this centreline and the photodetector (b) was 390 mm.

The schematic representation for GCLAD-B is illustrated in Fig. 8. The laser beam was positioned parallel to the wave refracted in the air on the vertical plane containing the specimen's longitudinal centerline. Thus, the angle between the specimen surface and the laser beam was 6.7° . The photodetector was at a distance of 120 mm from the specimen.

The employed laser was a TOPTICA iBeam Smart 640, with a power of 5 mW, wavelength equal to 640 nm, and beam collimated on a 1.2 mm x 0.7 mm elliptical spot (measured by a beam profiler at the device's output). The employed photodiode for the GCLAD photodetector is a Red Enhanced Quad Cell Silicon Photodiode (SD 197–23–21–014) developed by Luna Optoelectronics. The signal acquisition from the photodiode was synchronised with the excitation of the piezoelectric probe. Hence, the obtained signal was pre-processed with a Brüel & Kjær 2638 wideband signal conditioner. It applied a bandpass filter to isolate the frequencies from 300 kHz to 2 MHz. The final signal was the result of the average of 512 signals.

4. Results

Figs. 9 and 10 show the time-domain and the time-frequency domain signal relative to the specimen with a 6 mm deep and 30 mm wide defect, acquired with the interferometer and GCLAD-A.

The signals have been normalised with respect to the peak of their envelope to have signals contained in the normalised amplitude band

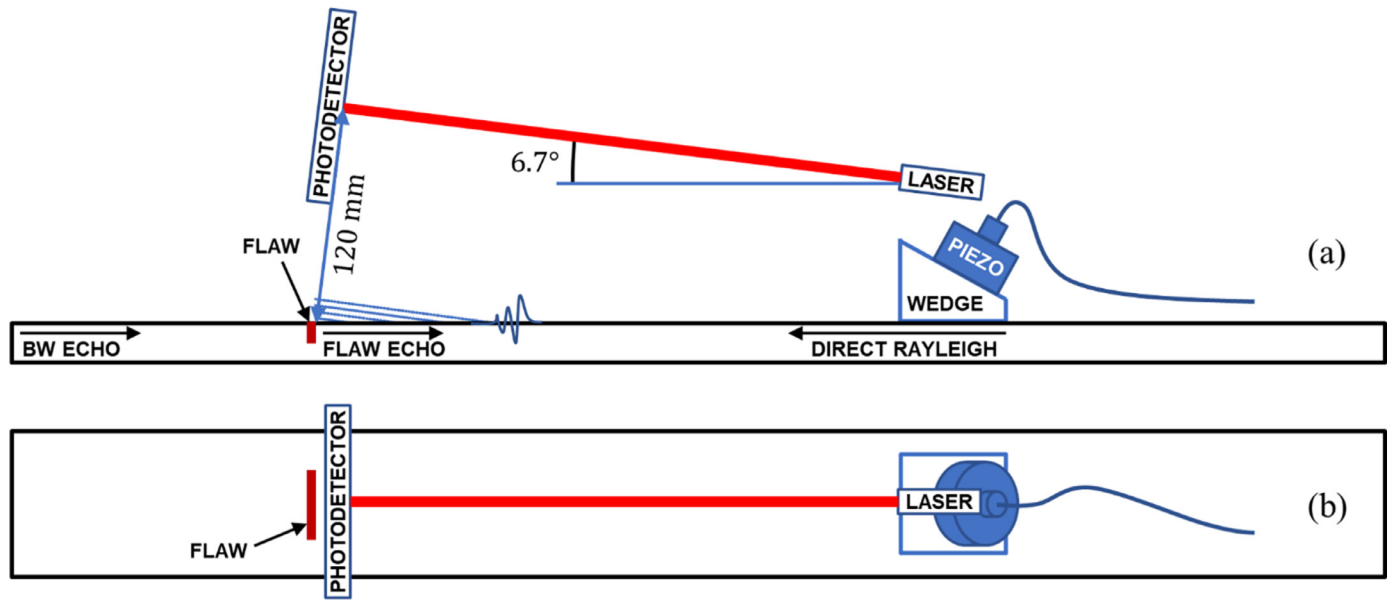


Fig. 8. Schematic representation of the experimental setup used for GCLAD-B. Side view (a) and top view (b).

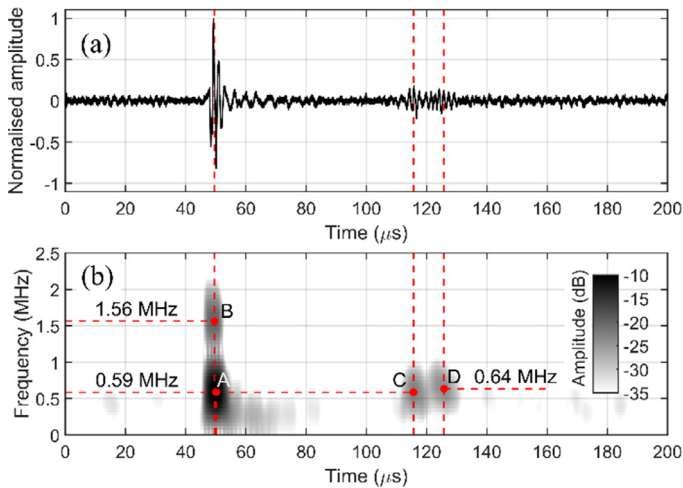


Fig. 9. Interferometric signal relative to the specimen with a 6 mm deep and 30 mm wide defect, acquired at 100 mm from the defect. Time-domain signal (a) and time-frequency domain signal (b).

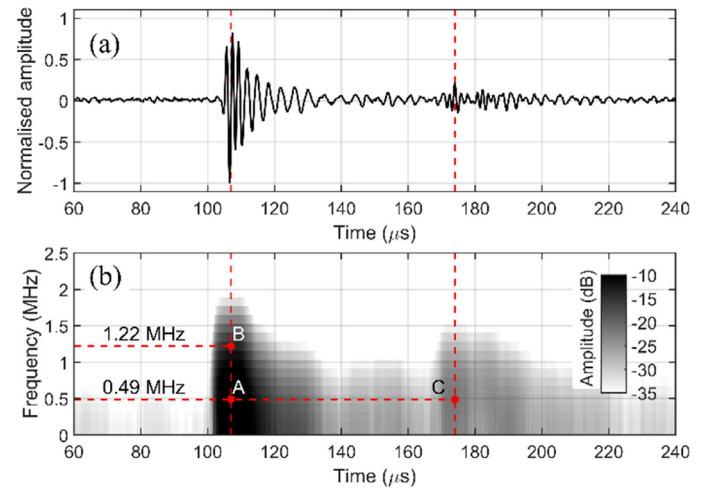


Fig. 10. GCLAD-A signal relative to the specimen with a 6 mm deep and 30 mm wide defect, acquired at 100 mm from the defect. Time-domain signal (a) and time-frequency domain signal (b).

comprised between ± 1 , which allows comparing their counterpart in the time-frequency domain. The piezoelectric probe, coupled with the specimen surface through a perspex wedge and coupling gel, generates a lobe that mainly propagates surface Rayleigh waves and minor transverse (shear) waves in the specimen. The transverse waves, being the specimens of small thickness, propagate over the entire thickness and are reflected by the bottom surface of the specimen. It must be noted that there might also be Lamb waves, which propagate at different speeds depending on the frequency. The wave oscillations with lower frequency content, which are seen immediately after the peak of the direct wave, could just be related to a Lamb wave. Thus, the consequent mode conversions and echoes interfere with the surface waves. In Fig. 9, the first signal peak relates to the direct surface wave for the interferometric signal. It has the maximum frequency content in point A (at 0.59 MHz) and a secondary frequency lobe with a maximum at a higher frequency (point B, at 1.56 MHz). Beyond the probe's frequency bandwidth, this latter frequency lobe is thought to be the result of the interference between the surface wave and the shear wave; the latter is evidenced in this

thin specimen because a part of the shear wave reflects on the bottom surface of the specimen, reaches the detection point, and then reflects on the defect. Indeed, it has been observed that the interference between waves generates spurious frequencies in the detected signal. The following two visible signal peaks are echoes generated by the defect, i.e., both surface and shear components. They are very close to each other and may partially overlap at particular distances from the defect. Their maximum frequency content is at 0.59 MHz and 0.64 MHz, respectively (see points C and D, in Fig. 9). In Fig. 10, relative to the GCLAD signal, the first signal peak has the maximum frequency content in point A (at 0.49 MHz) and a secondary frequency lobe with a maximum at a higher frequency (1.22 MHz at point B). Only one echo generated by the defect is clearly distinguishable along the signal after the direct wave, with maximum frequency content at 0.49 MHz (see point C, in Fig. 10). Comparing the signals in time and in the time-frequency domain shows that, whereas the interferometric measurement can detect higher frequencies, the GCLAD technique responds better to low frequencies. GCLAD is more sensitive to low frequencies, which gives rise

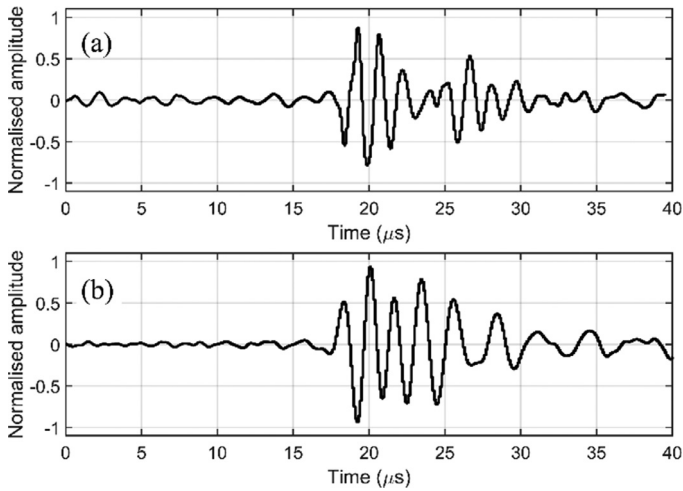


Fig. 11. Echo signals relative to the sample with a 1 mm deep and 10 mm wide defect, collected at a distance of 100 mm from the defect. Interferometric signal (a) and GCLAD-A signal (b). The time windows are centred around the waves' arrival time, for an easy comparison.

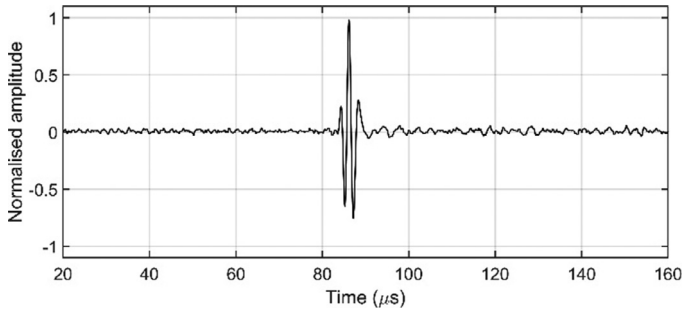


Fig. 12. Surface wave signal collected through the GCLAD-A technique from a 60 mm thick sample (SNR = 27.3).

to wave trains with longer tails. That increases the dead zone and reduces the detectability of the surface wave echo. Fig. 11 compares the echo signals (i.e., sequence of surface and shear waves) acquired by the two systems at 100 mm from the defect. The first peak of the surface echo signal is distinguishable for the interferometric signal, while for the GCLAD system, the surface echo signal and the shear echo signal partially overlap, making detection more difficult.

For a thicker specimen, where no signal overlap occurs because the shear wave echo is not present, the GCLAD responds well. For example, Fig. 12 shows a signal acquired with GCLAD-A on a 60 mm thick sample. There, the interference is not present, and the signal appears concentrated in a narrow time window, with a band centred on that of the piezoelectric probe, thanks to the higher thickness of the sample.

Referring to the background noise level in the signal measured before the rise of the direct wave, the interferometric signals show a low signal-to-noise for both the direct wave and the defect echo (e.g. in Fig. 9, direct wave SNR = 12.5 and defect echo SNR = 2.8). These low SNR values are caused by the rough surface of the specimens (refer also to Fig. 5), which hampers the interferometric measurement. The signals acquired with the GCLAD system are less affected by noise, as the system detects the wave in the air and is less sensitive to the surface finish of the test piece (e.g., for the signal in Fig. 10, direct wave SNR = 23.6 and defect echo SNR = 4.7). In order to mitigate the effect of amplification of low frequencies compared to high frequencies, observed in the GCLAD system, the interference between different waves and increase the SNR in the interferometric signals, a 0.4–1.2 MHz bandpass filter was applied to all signals in all subsequent analyses.

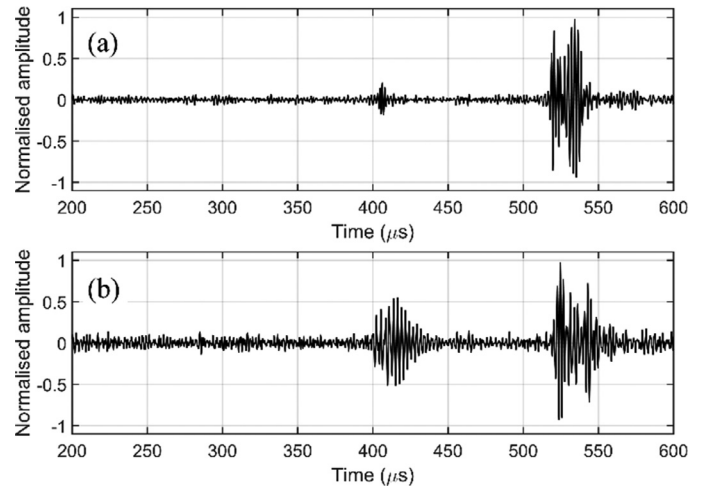


Fig. 13. GCLAD-B signal filtered with a 0.4–1.2 MHz bandpass filter, acquired from the specimen with a 1 mm x 10 mm defect (echo SNR = 3.17) (a) and from the specimen with 6 mm x 30 mm defect (echo SNR = 4.08) (b).

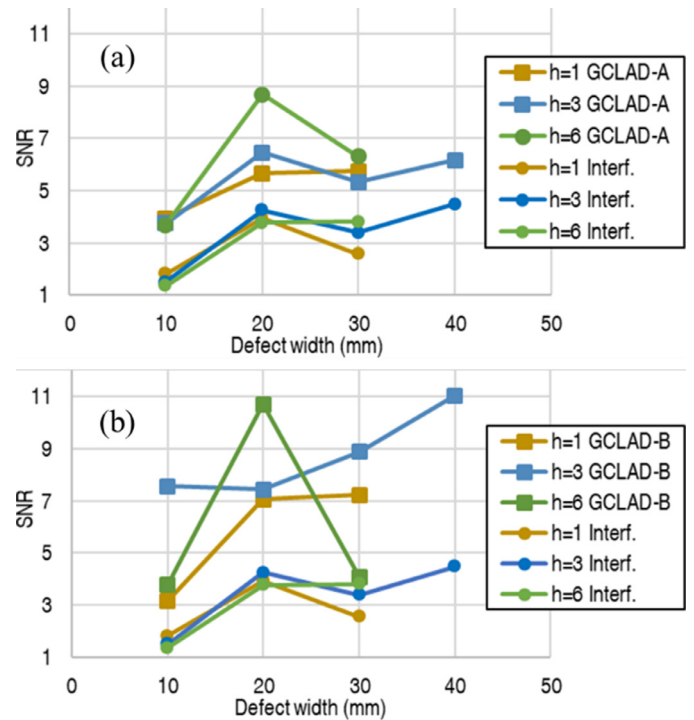


Fig. 14. SNR of signals acquired at 100 mm from the defect, with the interferometer and GCLAD-A (a) and GCLAD-B (b).

In the GCLAD-B measurement system, since the laser beam is perpendicular to the direction of propagation of the echoes of the ultrasonic signal, the direct signal is not detected. Therefore, the acquired signals contain the defect echo and the echo from the bottom surface of the specimen. Fig. 13a shows the GCLAD-B signal relative to the tiniest defect (1 mm x 10 mm) amongst those tested.

Fig. 13b shows the GCLAD-B signal for the 6 mm x 30 mm defect. The defect echo has SNR=4.08. In this case, the echo produced by the specimen bottom surface has a much lower amplitude than those relative to the 1 mm x 10 mm defect since most of the ultrasonic wave energy is reflected by the defect. It is also observed that the defect echo, as well as the echo originating from the extremity of the specimen, is characterised by the partial overlap of two echoes (i.e., surface and shear component) caused by the small thickness of the specimens. This phenomenon causes

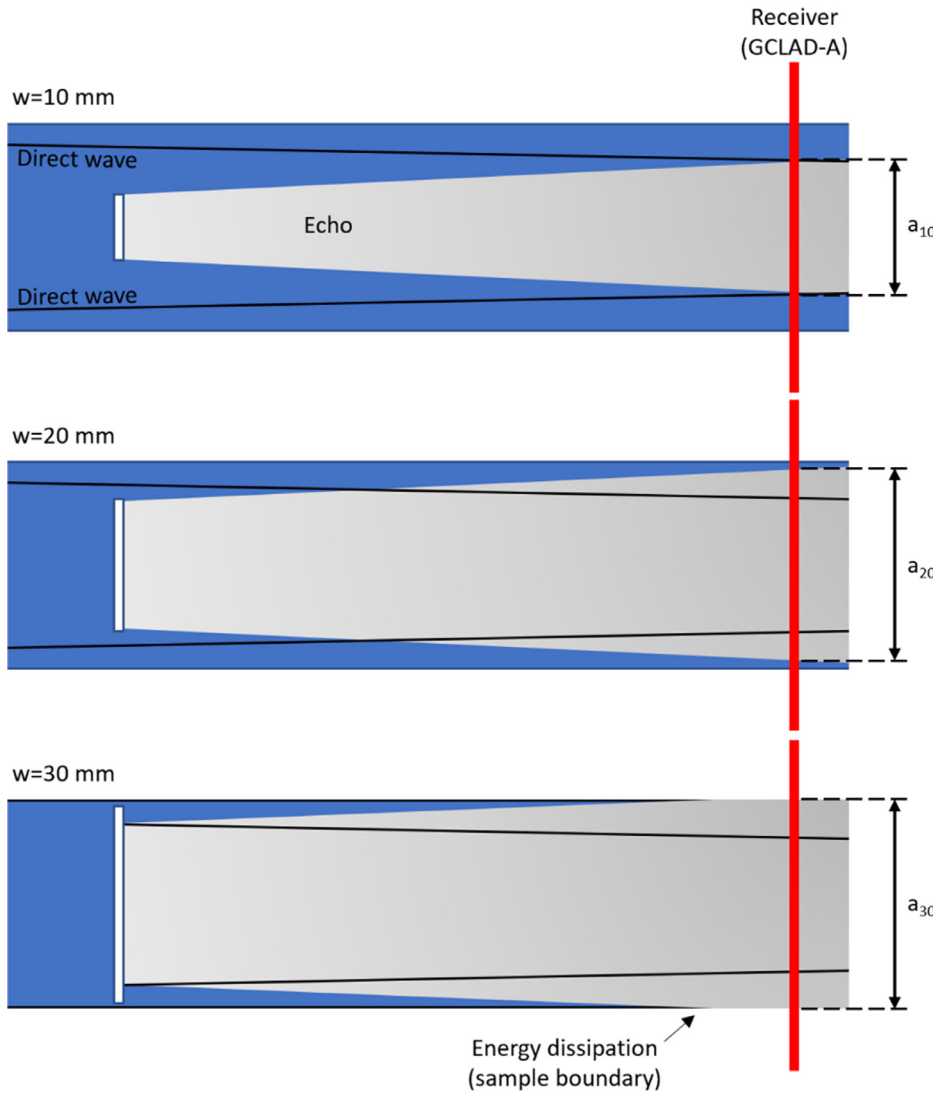


Fig. 15. Visualisation of the ultrasonic echo propagation in the sample for different values of sample thickness w .

interference that undoubtedly results in amplitude variations, making the amplitude of the defect echo not always linear and predictable as its size varies.

Fig. 14a compares the SNRs of the signals acquired interferometrically and with the GCLAD-A system at 100 mm from the defect, as the size of the defects varies. The trends are similar and show a maximum response for the 20 mm wide defects. A similar comparison is shown for the GCLAD-B system in Fig. 14b. In this last case, the interferometric measurements were carried out at 100 mm from the defect, while the GCLAD system measured over the entire space between the piezoelectric probe and the defect.

The trend for GCLAD-B is different from the GCLAD-A one. This can depend on several aspects, i.e., the sample geometry and the defect shape. In fact, based on this latter element, the wavefront propagating in air has a peculiar profile, with a specific curvature [40]. The GCLAD-A averages the oscillations from several wave crests being hence relatively insensitive to irregularities in the defect profile. Conversely, the GCLAD-B response is strongly affected by the position of the intersection point between the defect profile and the plane that contains the laser beam [40]. Because of the complex interaction with the geometry of both sample and defect, this aspect will be investigated by Finite Element simulations in dedicated future research.

Fig. 15 provides a visualisation of the phenomenon that leads to the maximum amplitude observed in Fig. 14 for a defect width w of 20 mm.

The defect always behaves as an ultrasonic source when it is subjected to the travelling direct wave, emitting an echo that diverges in the far field; regarding the reception, the GCLAD-A has been considered in the figure for convenience, but the same applies to other types of receivers. In the case of $w = 10$ mm and neglecting scattering along the path, the echo reaches the receiving position with an energy that is proportional to the width of the defect but whose density is inversely proportional to the length a_{10} (as the energy distributes with distance). The same applies to the case of $w = 20$ mm, but here the energy density at the detection point is higher for two reasons: the defect width is higher, and the ratio between a_{20} and w is lower (the energy is distributed in a narrower area compared to the case of $w = 10$ mm). Finally, for $w = 30$ mm, the divergence of the echo is such that the full width of the specimen is covered during the travel towards the receiving point (a_{30} equals the specimen width) so that consistent energy dissipation occurs because of interaction with air at the sample boundary and a consequent decrease in SNR is observed.

Fig. 16 shows the SNR trend of the peak due to the defect, for the two measurement systems, as the distance of the measurement point from the defect increases. For values of the measurement distance from the defect of less than 20 mm, the GCLAD system does not allow to distinguish the echo of the defect due to the overlap with the direct signal. The figure also shows the SNR value obtained with GCLAD-B, independent of the measurement distance due to the measurement method.

Table 2
Summary of the experimental findings.

	Interferometric method	GCLAD-A	GCLAD-B
Detection ability	↑	↑	↑
Spatial resolution	↑	↔	↔
Reception band	↑	↔	↔
SNR	↔	↑	↑
Sensitivity to surface roughness	↑	↓	↓
Amplitude decreasing vs reflector distance	↔	↔	not applicable
Scan size	spot	line	line
Portability	↔	↔	↔
Applicability in the industrial field	↑	↑	↑
Possibility of being automated	↑	↑	↑
Costs	↑	↓	↓

Legend: ↑ = high; ↔ = medium; ↓ = low.

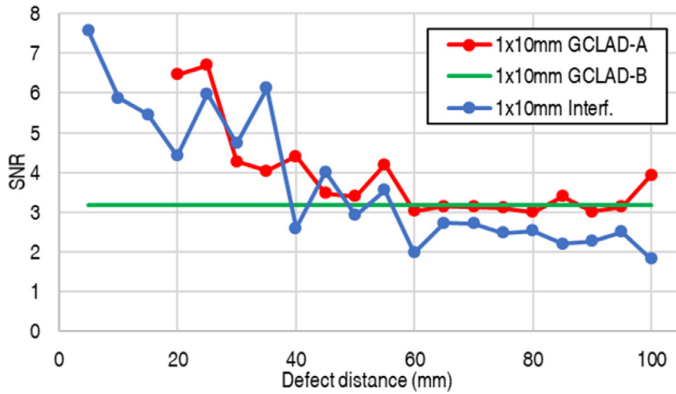


Fig. 16. SNR of signals acquired with the interferometer and GCLAD as the distance of the measurement point from the defect increases.

The obtained results should be considered as a qualitative tool for comparing the analysed techniques: it is clear that the reported trends for the received signals are dependant on the sample geometry and different ultrasonic patterns could be evidenced in diverse specimens. Nevertheless, the comparison between the two systems allows the following observations to be drawn:

- Both systems detected all artificial defects;
- The interferometer has a wide reception band and allows the reception of echoes distributed over very narrow time windows, with a limited dead zone and excellent spatial resolution. The defects are detected even when the measurement points are very close to the defect itself;
- GCLAD has a narrower frequency band. The high-frequency signal components are attenuated, generating partial overlaps and interference that can limit the resolution in space. It happens when the echoes are close to each other, as in the low-thickness specimens used in this work. Therefore, defects very close to the measuring point are not easily detectable;
- SNR is generally better for the GCLAD-A and GCLAD-B than for the interferometer. For the interferometric technique, the SNR depends on surface reflectivity and roughness. The GCLAD system is much less influenced by the roughness and state of the surface of the piece since it detects the acoustic wave in the air;
- GCLAD-A and GCLAD-B provide comparable results in terms of SNR, with the parameters used described in Section 2.2;
- The amplitude of the signal, for both methods, decreases comparably as the distance of the measurement point from the defect increases due to the attenuation of the ultrasound wave in the piece;
- The SNR trends for the investigated dimensions of the defects do not follow a precise logic, as the specimens' limited dimensions greatly influence them. The specimen side surfaces cause partial overlaps

between different echoes, not only of surface waves, resulting in destructive and constructive interference effects;

- Another substantial difference between the two detection methods is that the interferometer makes a point measurement, while GCLAD makes a line measurement. Depending on the application, these characteristics can make one or the other technique more suitable. Additional considerations on dimensions, portability, applicability, and costs include the following points.
- A rigid and bulky chassis is needed for precise beam collimation in the interferometric equipment. However, since the optical head can be connected via optic fibre to the chassis, it is still flexible and versatile, guaranteeing the inspection of areas difficult to access. For the GCLAD technique, it is necessary to have a rigid connection between the laser source or the optical head and the photodiode to avoid mutual movement. Therefore, a rigid structure is required, which can be cumbersome for part inspection. To have good sensitivity, the distance between the laser source and photodiode must be high, in the order of a few tens of centimetres, depending on the diameter and divergence of the laser beam. However, it is possible to adopt multipass cell systems to lengthen the optical path while maintaining a small footprint [40].
- An interferometric UT inspection setup can be considered pricier than the GCLAD, but the higher detectable frequency allows characterisations of smaller defects. Moreover, the evolution of interferometric technology leads to higher acquisition frequency; thus, a levelling of the price for more conventional apparatus is expected. Using a collimated laser beam probe with a small diameter allows the GCLAD system to obtain a higher bandwidth, sufficient for the routine inspection of mechanical parts. The technique can be used in a tank with a liquid instead of air, obtaining a bandwidth of over 15 MHz.

The findings of the experimental results are summarised in Table 2.

5. Conclusions and future work

This work proposed using interferometric and deflectometry laser-based methods to record ultrasonic waves generated by a piezoelectric probe. The employed interferometry method is based on multi-signal homodyning. The deflectometry approach is based on Gas-Coupled Laser Acoustic Detection (GCLAD). The present work conducted a direct comparison of the two techniques. Specimens with artificial flaws of different depths and widths were used as common testpieces. The experimental outcomes show the advantages and drawbacks of the two measurement approaches and allow drawing the following remarks:

- Both methods have great potential to be applied in industrial fields, considering that both can be automated, are contactless, independent from the material to be analysed and allow the fast evaluation of significant components;
- The interferometric method provides higher spatial resolution than GCLAD;

- Whereas the interferometric approach is suited to measure ultrasonic waves on smooth and reflective surfaces, GCLAD is capable of detecting ultrasonic waves on rough surfaces;
- Some concerns are still related to the cost of the equipment, particularly for the interferometric method.

Future research should focus on further characterising the two methods, using thicker sample geometries that minimise the wave interference phenomena. An extended evaluation of the dependence of the sensitivity on different flaw types and different surface roughness values is also desirable. Moreover, numerical analyses should be performed to fully understand how the specimen's geometry, defect shape, wave propagation, and wave interference phenomena influence the performance of the two non-contact measurement methods.

Funding

Part of the research has been performed in the context of the MAGNUM project (Macchinario per l'ispezione Automatizzata di asili ferroviari basata sulla Generazione Nonconvenzionale di Ultrasuoni tramite Metodologie laser), funded by Regione Toscana under Grant Agreement #3553.04032020.158000322.

Declaration of Competing Interest

The authors declare that they have no known competing financial interests or personal relationships that could have appeared to influence the work reported in this paper.

CRediT authorship contribution statement

D. Vangi: Conceptualization, Software, Formal analysis, Investigation, Resources, Writing – original draft, Supervision, Project administration. **M.S. Gulino:** Methodology, Formal analysis, Resources, Data curation, Writing – review & editing, Visualization. **N. Montinaro:** Methodology, Formal analysis, Investigation, Writing – review & editing, Visualization. **C. Mineo:** Conceptualization, Software, Formal analysis, Investigation, Writing – original draft, Visualization. **D. Cerniglia:** Conceptualization, Formal analysis, Investigation, Resources, Supervision. **G. Epasto:** Conceptualization, Methodology, Formal analysis, Writing – original draft, Writing – review & editing.

Data availability

Data will be made available on request.

References

- [1] Green RE. Non-contact ultrasonic techniques. *Ultrasonics* 2004;42:9–16. doi:10.1016/j.ultras.2004.01.101.
- [2] Lee J-R, Shin H-J, Chia CC, Dhital D, Yoon D-J, Huh Y-H. Long distance laser ultrasonic propagation imaging system for damage visualization. *Opt Lasers Eng* 2011;49:1361–71. doi:10.1016/j.optlaseng.2011.07.011.
- [3] Yang C-H, Jeyaprasanth N, Hsu Y-W. Applicability of non-destructive laser ultrasound and non-linear ultrasonic technique for evaluation of thermally aged CF8 duplex stainless steel. *Int J Press Vessel Pip* 2021;193:104451. doi:10.1016/j.jipvp.2021.104451.
- [4] Cantrell JH, Salama K. Acoustoelastic characterisation of materials. *Int Mater Rev* 1991;36:125–45. doi:10.1179/imr.1991.36.1.125.
- [5] Chimenti DE. Review of air-coupled ultrasonic materials characterization. *Ultrasonics* 2014;54:1804–16. doi:10.1016/j.ultras.2014.02.006.
- [6] Scruby CB, L. D. *laser ultrasonics techniques and applications*. CRC Press; 1990.
- [7] Gulino M-S, Bruzzi M, Vangi D. Gas-coupled laser acoustic detection technique for NDT of mechanical components. *Ultrasonics* 2021;114:106415. doi:10.1016/j.ultras.2021.106415.
- [8] Li Y, Fu Y, Ji Z, Li X, Ji Y, Zheng X, et al. Single-wired array light detector based on photoacoustic effect. *Opt Lasers Eng* 2021;139:106460. doi:10.1016/j.optlaseng.2020.106460.
- [9] Wissmeyer G, Pleitez MA, Rosenthal A, Ntziachristos V. Looking at sound: optoacoustics with all-optical ultrasound detection. *Light Sci Appl* 2018;7:53. doi:10.1038/s41377-018-0036-7.
- [10] Monchalain J-P. Optical detection of ultrasound. *IEEE Trans Ultrason Ferroelectr Freq Control* 1986;33:485–99. doi:10.1109/T-UFFC.1986.26860.
- [11] Calder CA. Noncontact material testing using laser energy deposition and interferometry. *Mater Eval* 1980;38:86–91.
- [12] Monchalain J-P. Progress Towards the Application of Laser-Ultrasonics in Industry. In: *Rev. prog. quant. nondestruct. eval*. Boston, MA: Springer US; 1993. p. 495–506. doi:10.1007/978-1-4615-2848-7_64.
- [13] Wagner JW. Optical detection of ultrasound. *Phys Acoust* 1990;19:201–66.
- [14] DEWHURST RJ. Optical sensing of ultrasound. *Nondestruct Test Eval* 1990;5:157–69. doi:10.1080/10589759008952962.
- [15] Dewhurst R.J. Optical ultrasonic sensors for monitoring from industrial surfaces. In: Gorecki C, Preater RWT, editors., 1994, p. 106–15. doi:10.1117/12.194309.
- [16] Royer D, Noroy M-H, Fink M. Optical generation and detection of elastic waves in solids. *Le J Phys IV* 1994;04 C7-673-C7-684. doi:10.1051/jp4:19947159.
- [17] Asher RC. Ultrasonic sensors for the process industry. *Meas Control* 1997;30:138–40. doi:10.1177/002029409703000503.
- [18] Dewhurst RJ, Shan Q. Optical remote measurement of ultrasound. *Meas Sci Technol* 1999;10:R139–68. doi:10.1088/0957-0233/10/11/201.
- [19] Noui L, Dewhurst RJ. A laser beam deflection technique for the quantitative detection of ultrasonic Lamb waves. *Ultrasonics* 1993;31:425–32. doi:10.1016/0041-624X(93)90051-Z.
- [20] Dewhurst RJ, Williams BA. A study of lamb wave interaction with defects in sheet materials using a differential fibre-optic beam deflection technique. *Mater Sci Forum* 1996;210–213:597–604. doi:10.4028/www.scientific.net/MSF.210-213.597.
- [21] Barnes RA, Maswadi S, Glickman R, Shadaram M. Probe beam deflection technique as acoustic emission directionality sensor with photoacoustic emission source. *Appl Opt* 2014;53:511. doi:10.1364/AO.53.000511.
- [22] Dewhurst RJ, Williams BA. Fibre optic system for the monitoring of asymmetric Lamb wave modulation in thin films. *Electron Lett* 1997;33:1813. doi:10.1049/el:19971180.
- [23] Monchalain J-P. Laser-ultrasonics: from the laboratory to industry. In: *AIP Conf. Proc*. 700. AIP; 2004. p. 3–31. doi:10.1063/1.1711602.
- [24] Zhu X, Huang Z, Wang G, Li W, Zou D, Li C. Ultrasonic detection based on polarization-dependent optical reflection. *Opt Lett* 2017;42:439. doi:10.1364/OL.42.000439.
- [25] Marcantonio V, Monarca D, Colantoni A, Cecchini M. Ultrasonic waves for materials evaluation in fatigue, thermal and corrosion damage: a review. *Mech Syst Signal Process* 2019;120:32–42. doi:10.1016/j.ymssp.2018.10.012.
- [26] Montinaro N, Epasto G, Cerniglia D, Guglielmino E. Laser ultrasonics for defect evaluation on coated railway axles. *NDT E Int* 2020;116:102321. doi:10.1016/j.ndteint.2020.102321.
- [27] Park B, Sohn H, Yeum C-M, Truong TC. Laser ultrasonic imaging and damage detection for a rotating structure. *Struct Heal Monit* 2013;12:494–506. doi:10.1177/1475921713507100.
- [28] An Y-K, Park B, Sohn H. Complete noncontact laser ultrasonic imaging for automated crack visualization in a plate. *Smart Mater Struct* 2013;22:025022. doi:10.1088/0964-1726/22/2/025022.
- [29] Montinaro N, Cerniglia D, Pitarresi G. Evaluation of vertical fatigue cracks by means of flying laser thermography. *J Nondestruct Eval* 2019;38:48. doi:10.1007/s10921-019-0586-5.
- [30] Zhang K, Zhou Z. Quantitative characterization of disbonds in multilayered bonded composites using laser ultrasonic guided waves. *NDT E Int* 2018;97:42–50. doi:10.1016/j.ndteint.2018.03.006.
- [31] Lee C, Park S. Damage visualization of pipeline structures using laser-induced ultrasonic waves. *Struct Heal Monit* 2015;14:475–88. doi:10.1177/1475921715596220.
- [32] Murfin AS, Soden RAJ, Hatrick D, Dewhurst RJ. Laser-ultrasound detection systems: a comparative study with Rayleigh waves. *Meas Sci Technol* 2000;11:1208–19. doi:10.1088/0957-0233/11/8/315.
- [33] Diaci J. Transfer function of the laser beam deflection probe for detection of cylindrical acoustic waves in a transverse arrangement. *Le J Phys IV* 1994;04:C7-773-C7-776. doi:10.1051/jp4:19947182.
- [34] Caron JN, Mehl JB, Steiner KV. Ultrasonic NDE of composite panels with gas-coupled laser acoustic detection. In: *Rev. prog. quant. nondestruct. eval*. Boston, MA: Springer US; 1998. p. 635–42. doi:10.1007/978-1-4615-5339-7_82.
- [35] Caron JN. Displacement and deflection sensitivity of gas-coupled laser acoustic detection. *1st Int. Symp Laser Ultrason Sci Technol Appl* 2008:1–6.
- [36] Caron JN, DiComo GP. Frequency response of optical beam deflection by ultrasound in water. *Appl Opt* 2014;53:7677. doi:10.1364/AO.53.007677.
- [37] Caron JN, Kunapareddy P. Atypical applications for gas-coupled laser acoustic detection. *J Phys Conf Ser* 2014;520:012022. doi:10.1088/1742-6596/520/1/012022.
- [38] Gulino M-S, Bruzzi M, Vangi D. Application of the Gas-Coupled Laser Acoustic Detection technique to non-destructive monitoring of mechanical components. *J Phys Conf Ser* 2021 1977:012006. doi:10.1088/1742-6596/1977/1/012006.
- [39] Vangi D, Bruzzi M, Caron JN, Gulino M-S. Crack detection with gas-coupled laser acoustic detection technique. *Meas Sci Technol* 2021;32:095202. doi:10.1088/1361-6501/abfced.
- [40] Vangi D, Bruzzi M, Caron JN, Gulino MS. Compact probe for non-contact ultrasonic inspection with the gas-coupled laser acoustic detection (GCLAD) technique. *Exp Mech* 2022;62:403–15. doi:10.1007/s11340-021-00786-7.
- [41] Vangi D, Bruzzi M, Caron JN, Gulino MS. Signal enhancement in surface crack detection with gas-coupled laser acoustic detection. *J Nondestruct Eval* 2021;40:85. doi:10.1007/s10921-021-00820-7.
- [42] Gulino M-S, Bruzzi M, Caron JN, Vangi D. Non-contact ultrasonic inspection by gas-coupled laser acoustic detection (GCLAD). *Sci Rep* 2022;12:87. doi:10.1038/s41598-021-04191-x.
- [43] Koukoulas T, Robinson S, Rajagopal S, Zeqiri B. A comparison between heterodyne and homodyne interferometry to realise the SI unit of acoustic pressure in water. *Metrologia* 2016;53:891–8. doi:10.1088/0026-1394/53/2/891.

- [44] Blum TE, van Wijk K, Pouet B, Wartelle A. Multicomponent wavefield characterization with a novel scanning laser interferometer. *Rev Sci Instrum* 2010;81:073101. doi:[10.1063/1.3455213](https://doi.org/10.1063/1.3455213).
- [45] Pouet B. Robust laser-ultrasonic interferometer based on random quadrature demodulation. In: *AIP Conf. Proc.*, 820. AIP; 2006. p. 233–9. doi:[10.1063/1.2184534](https://doi.org/10.1063/1.2184534).
- [46] McKenzie K, Gray MB, Lam PK, McClelland DE. Technical limitations to homodyne detection at audio frequencies. *Appl Opt* 2007;46:3389. doi:[10.1364/AO.46.003389](https://doi.org/10.1364/AO.46.003389).
- [47] Fritschel P, Evans M, Frolov V. Balanced homodyne readout for quantum limited gravitational wave detectors. *Opt Express* 2014;22:4224. doi:[10.1364/OE.22.004224](https://doi.org/10.1364/OE.22.004224).
- [48] Tanaka K, Ohtsuka Y. Effects of surface roughness of a moving test body on laser-interferometric displacement measurements. *Opt Commun* 1975;14:110–14. doi:[10.1016/0030-4018\(75\)90070-X](https://doi.org/10.1016/0030-4018(75)90070-X).
- [49] Wang Y, Wolfe WL. Scattering from microrough surfaces: comparison of theory and experiment. *J Opt Soc Am* 1983;73:1596. doi:[10.1364/JOSA.73.001596](https://doi.org/10.1364/JOSA.73.001596).
- [50] Holzer JA, Sung CC. Scattering of electromagnetic waves from a rough surface. II. *J Appl Phys* 1978;49:1002–11. doi:[10.1063/1.325037](https://doi.org/10.1063/1.325037).
- [51] Zeng Y, Wang X, Qin X, Hua L, Xu M. Laser ultrasonic inspection of a wire + Arc additive manufactured (WAAM) sample with artificial defects. *Ultrasonics* 2021;110:106273. doi:[10.1016/j.ultras.2020.106273](https://doi.org/10.1016/j.ultras.2020.106273).
- [52] Cerniglia D, Scafidi M, Pantano A, Rudlin J. Inspection of additive-manufactured layered components. *Ultrasonics* 2015;62:292–8. doi:[10.1016/j.ultras.2015.06.001](https://doi.org/10.1016/j.ultras.2015.06.001).
- [53] Maswadi SM, Ibey BL, Roth CC, Tsybouski DA, Beier HT, Glickman RD, et al. All-optical optoacoustic microscopy based on probe beam deflection technique. *Photoacoustics* 2016;4:91–101. doi:[10.1016/j.pacs.2016.02.001](https://doi.org/10.1016/j.pacs.2016.02.001).